Molecular Dynamics Simulation of the Cation Motion upon Adsorption of CO_2 in Faujasite Zeolite Systems

D. F. Plant,[†] G. Maurin,*[,†] H. Jobic,[‡] and P. L. Llewellyn[§]

Laboratoire LPMC, UMR CNRS 5617, Université Montpellier II, Pl. E. Bataillon, 34095 Montpellier Cedex 05, France, Institut de Recherches sur la Catalyse, CNRS, 2 Avenue Albert Einstein, 69626 Villeurbanne, France, and Laboratoire MADIREL, CNRS Université de Provence (UMR 6121), Centre Saint Jérôme, Avenue Escadrille Normandie Niemen, 13397 Marseille Cedex 20, France

Received: April 18, 2006; In Final Form: May 31, 2006

Molecular Dynamics simulations have been carried out in NaX and NaY Faujasite systems to deepen understanding of the cation rearrangement during the CO2 adsorption process suggested by our recent diffusivity measurements. This study is a major contribution since the rearangement of the cations in Faujasite, the most promising adsorbent for CO_2 storage, can represent a significant breakthrough in understanding the adsorption and diffusion processes at the mircroscopic scale. For NaY, it has been shown that at low and intermediate loadings, SII cations can migrate toward the center of the supercage due to strong interactions with the adsorbates, followed by a hopping of SI′cation from the sodalite cage into the supercage to fill the vacant SII site. The SI cations are only displaced at a higher loading, leading to cation de-trapping out of the double six rings into the vacant SI′ sites. For NaX, the SIII′ cations which occupy the most accessible adsorption sites move significantly upon coordination to the carbon dioxide molecules. The SI′ and SII cations remain consistently located in their initial sites whatever the loading. Indeed, the most probable migration mechanism involves SIII′ cation displacements into nearby vacant SIII′ sites.

1. Introduction

Carbon dioxide is a strategic gas in many industrial processes. As both a product of combustion and a significant greenhouse gas, its recovery and elimination/reuse is a major problem facing today's society[1]. One solution to recover carbon dioxide is to employ an adsorption process. Well ordered microporous systems such as the zeolite family[2] are among the potential materials for the selective adsorption and separation of carbon dioxide.[3,4] They are of great interest because of the possibility to fine-tune their properties which influence the adsorption performance either from a textural point of view (pore size, pore architecture) or from a chemical point of view (e.g., Si/Al ratio and nature of the extraframework cations[5,6]). It has been previously reported that narrow pore size zeolites such as Na-4A[7] and CaA[8] are most suitable for pressure swing adsorption (PSA)-based system.[9] More recently, a study based on an exhaustive zeolite adsorbent screening reported that the most promising adsorbents for carbon dioxide sequestration are characterized by a low Si/Al ratio and contain extraframework cations that give strong electrostatic interactions with carbon dioxide.[10] For given operating conditions corresponding to low-pressure carbon dioxide feed and regeneration, 13X and NaY are claimed to be the most suitable adsorbents.[10]

Knowledge of the location and distribution of extraframework cations in the zeolite systems is therefore crucial, since it influences the distribution of the electron density in the framework[11] and hence the interactions with the adsorbed molecules, leading to possible changes in the adsorption and separation properties of the cation exchanged zeolites.[5,12] Recent research efforts have been devoted to studying the migration of extraframework cations when adsorbing or desorbing water molecules.[13−20] We previously reported a redistribution of the cations in Na−Mordenite zeolite system upon water adsorption by combining dielectric relaxation spectroscopy and energy minimization techniques.[13] Similar behavior has also been reported in different zeolite systems, including Faujasite,[14−18] 4A,[19] and Natrolite,[20] using experimental techniques and modeling approaches based on molecular dynamics and Monte Carlo simulations. In NaY Faujasite systems, the SI−SI′ cation redistribution was predicted, following a direct cation−water interaction within the sodalite cages, whereas SII cations surprisingly do not redistribute upon water adsorption.[15] Few articles have reported the evidence of the cation redistribution in dry zeolite−adsorbate systems, which can lead to possible changes in the adsorption properties due to the increasing accessibility of the cation adsorption sites. Previous studies, both experimental and computational, have focused on the adsorption of halocarbons in Faujasite systems.[11,21−25] Neutron scattering and X-ray diffraction studies have suggested that the SI′ cations in the sodalite cages migrate into the supercages upon adsorption of both CHF_2CHF_2[21] and $CFCl_3$.[23] Similar findings were reported by Sanchez-Sanchez et al.[22] using MAS NMR spectroscopy, indicating possible motion of the sodium ions upon $CHCl_3$ adsorption.[11,22] These experimental observations were confirmed by molecular dynamics simulations based on classical potentials for describing the interactions between the whole system.[24,25] These authors reported concerted cation motion which involved jumps between SI, SI′, SII, and SII′ sites. We have also shown that the carbon dioxide adsorbates induce such a redistribution of the extraframework cations in NaY.

We recently modeled the diffusion of carbon dioxide in both NaX and NaY Faujasite systems using molecular dynamics

* To whom correspondence should be addressed: gmaurin@lpmc.univ-montp2.fr
[†] Université Montpellier II.
[‡] Institut de Recherches sur la Catalyse.
[§] CNRS Université de Provence.

10.1021/jp062381u CCC: $33.50
Published on Web 06/30/2006

(MD) simulations which were directly compared to our quasi-elastic neutron scattering (QENS) measurements[26,27] and previously PFG NMR reported data.[28] We have reported that the simulated diffusivities of CO_2 and the corresponding activation energies reproduce well the experimental data only when one takes into account the mobility of the cations. It was thus shown that the activation energies for both systems are about 30% higher when the cations are maintained fixed in their initial crystallographic sites.[27] As far as we know, it was the first clear evidence that a concerted motion involving the cations and the adsorbate molecules occurs in such materials. Furthermore, the originality of our previous study was to combine experimental and theoretical tools to quantitatively estimate the influence of the cation mobility on the adsorbates diffusivity. Here, an exhaustive series of MD simulations were performed to gain further understanding of the cation redistribution occurring upon the carbon dioxide adsorption in both Faujasite systems for several loadings. This study constitutes a major contribution since the rearangement of the cations in NaY and NaX, the most promising adsorbents for CO_2 storage, represents a significant breakthrough in understanding the adsorption and diffusion processes at the mircroscopic scale. Our simulations are mainly based on our previous validated interatomic potentials[29] assuming only physisorption in the zeolite−adsorbate system. This assumption is clearly supported by the previously reported experimental data.[30−32] Simulations are performed at 400 K over long simulation times allowing us to estimate both the mean square displacements (MSD) and the (cation−carbon dioxide) radial distribution functions (RDFs) for the different type of cation sites for a wide range of loadings from 21 to 78 and 25 to 92 CO_2 molecules per unit cell for NaX and NaY, respectively. These loadings correspond to those experimentally investigated by our previous QENS experiments.[26] We are thus able to provide the cation migration mechanisms in both NaX and NaY systems and show their dependence of the adsorbate loading

2. Computational Methodology

The crystal structures of the two Faujasite systems were modeled as follows. The chemical composition $Si_{192-x}Al_xNa_xO_{384}$ was considered with $x = 92$ and 56 in order to reproduce the experimental Si/Al ratios of 1.1 and 2.4 for NaX and NaY, respectively. The zeolite frameworks were built in accordance with Löwenstein's Al−O−Al avoidance rule.[33] The aluminum configurations representing NaY and NaX were then selected in order to reproduce the experimental cation distributions as one knows that the cation is embedded close to the aluminum position. The second step consisted of modeling the distribution of the extraframework cations among the different crystallographic sites described in Figure 1. The distribution for NaY was defined as follows, based on the structure refined from Neutron diffraction data by Fitch et al:[34] 6 cations in SI sites located in the center of the hexagonal prism connecting two sodalite cages, 18 in SI′ sites in the sodalite cage in front of the six-ring window connected to the hexagonal prism, and 32 in SII sites in 12-ring windows of the supercages. The sites occupied were chosen randomly around the aluminum positions, with the exception that neighboring SI and SI′ sites were not allowed to be occupied. For NaX, the distribution of the extraframework cations was taken from Zhu et al.[35] with 32 Na^+ in SI′ sites, 32 Na^+ in SII sites, 28 in SIII′ sites, six-ring and 12-ring windows of the supercages, respectively. In this later case, four positions from the initial 32 sites III′ were randomly removed. Both NaY and NaX structures were then

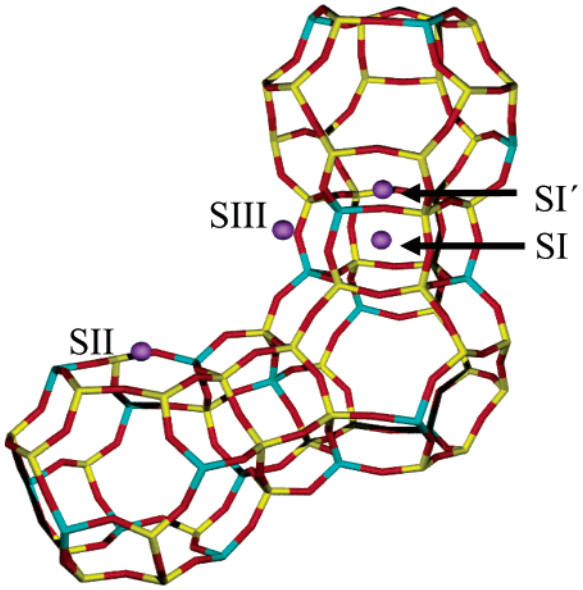

Figure 1. Molecular graphic representing the Faujasite-type zeolites structure with three sodalite cages connected by two hexagonal prisms. Description of the main crystallographic sites (SI, SI′, SII, and SIII′) for the extraframework cations.

energy-minimized with the GULP code,[36] using the force field developed by Ramsahye and Bell[25] and with the constraint that the cell remained cubic. The simulated cell parameters were only slightly modified by 0.08% and 0.10% compared to the experimental ones for NaY and NaX, respectively. The short-range interactions were described by Buckingham potentials, including explicit Si−O and Al−O terms, and additional harmonic three-body terms were defined for the O−Si−O and O−Al−O intratetrahedral angles to describe the flexibility of the framework. The Faujasite system is assumed to be semi-ionic with atoms carrying as previously reported[29] the following partial charges (in electron units): Si (+2.4), Al (+1.7), O_z (−1.2), and Na (0.7). The optimized geometries for both NaY and NaX showed that the cations remain located around their initial positions. These structures were then loaded with 21, 42, and 78 and 25, 50, 71, and 92 CO_2 molecules per unit cell for NaX and NaY, respectively, using the Sorption module in the Cerius^2 program.[37] These loadings were selected to mimic the experimental conditions used in our previous QENS experiments.[26] Prior to the molecular dynamics simulations, all the generated structures were optimized using GULP in order to provide the lowest-energy starting configurations.

The successful simulation of the cation redistribution upon adsorption of carbon dioxide in NaX and NaY systems required an accurate description of the interatomic potential between the carbon dioxide molecules and the zeolite framework, including the sodium cations, and between the adsorbate molecules. For carbon dioxide, we used an atomic point charge model where the molecules were free to alter their internal configurations and with the following charges (in electron units) assigned to the carbon C (+0.72) and the oxygen O (−0.36) atoms.[29] The adsorbate−zeolite framework and adsorbate−adsorbate repulsion−dispersion interactions were modeled using Lennard−Jones potentials with our previous parameters which successfully reproduced the adsorption properties of the purely siliceous Faujasite form.[38] The interaction between the extraframework cations and both the carbon and oxygen of carbon dioxide was modeled using Buckingham potentials we recently derived by ab initio cluster calculations.[39] The so-defined values of the A, ρ, and C parameters were slightly adjusted to reproduce the

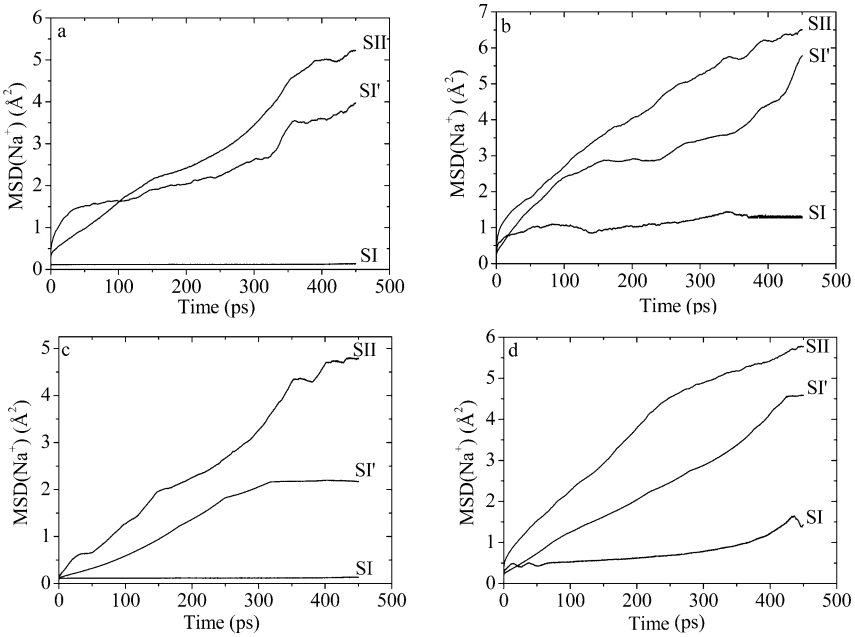

Figure 2. Mean square displacement (MSD) plots for the SI, SI′, and SII cations in NaY at 400 K and at loadings of (a) 25, (b) 50, (c) 71, and (d) 92 carbon dioxide molecules per unit cell.

TABLE 1: Buckingham Potential Parameters Used to Describe the Interactions between the Extraframework Cations and the Carbon Dioxide Molecules

	Buckingham potential $Ae^{-r/\rho} - C/r^6$		
ion pair	A (eV)	ρ (Å)	C (eV Å^6)
Na−C (CO_2)	576.0	3.120	0.0
Na−O (CO_2)	5600.0	4.421	31.8

differential enthalpies of adsorption at low coverage for NaX and NaY obtained by microcalorimetry.[29] This set of parameters is reported in Table 1.

These whole interatomic potentials were then implemented in the *DL_POLY* program[40] in the NVT ensemble using the Evans isokinetic thermostat.[41] We selected the optimized structures obtained by the minimization procedure as starting configurations and the minimized cell dimensions were kept fixed during the molecular dynamics (MD) runs. All components of the system (adsorbate and adsorbent) were then treated as fully flexible during the MD simulations. A time step of 1 fs was selected, with simulations run at the various loadings previously mentioned for NaX and NaY. The simulations were performed at 400 K, each for 10^6 steps (i.e., 1 ns), following 50 000 steps of equilibration. A short-range cutoff of 8.50 Å was used, while electrostatic interactions were evaluated using the Ewald method. The trajectory was recorded every 200 steps during the production stage, and radial distribution functions (RDF) were recorded every 500 steps. The mean square displacements (MSD) of each crystallographic type of extraframework cations for each loading were evaluated by means of the following equation:

$$\mathrm{MSD}(t) = \langle \Delta r_j^2(t) \rangle = \frac{1}{N}\sum_{j=1}^{N} \Delta r_j^2(t) = \frac{1}{N}\sum_{j=1}^{N} (r_j(t) - r_j(0))^2 \quad (1)$$

where N corresponds to the number of extraframework cations considered in the computation of the MSD, and we used multiple time origins in order to improve the statistics of the calculation. It is important to note that throughout this paper the labels SI, SI′, SII, and SIII′ for the cations refer to their location in the starting configuration and not to their position at any subsequent time.

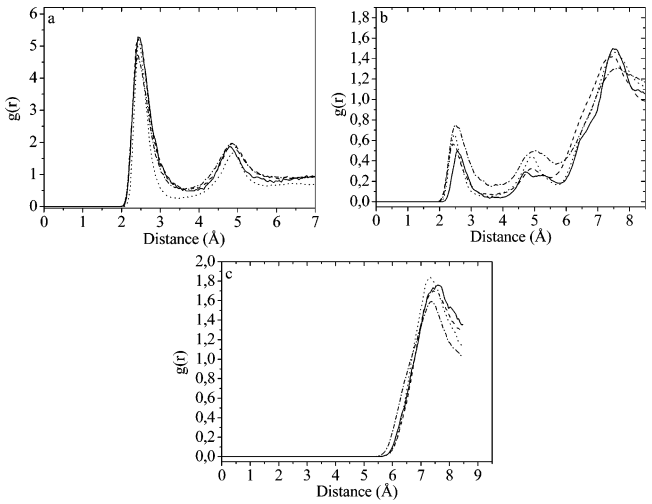

Figure 3. Radial Distribution Functions (RDFs) (a) Na^+(SII)-O(CO_2), (b) Na^+(SI′)-O(CO_2), and (c) Na^+(SI)−O(CO_2) for 25 (solid lines), 50 (dashed lines), 71 (dotted lines), and 92 (short dashed lines) carbon dioxide molecules per unit cell, calculated at 400 K for NaY/CO_2 system.

3. Results and Discussion

As previously reported,[25] when using the same force field to describe the zeolite framework, the Na^+ cations are essentially immobile in the bare NaY and NaX at 400 K during the MD run time scale. Figure 2 shows the MSD plots for the different cation sites in NaY at the various loadings investigated (25, 50, 71, and 92 CO_2 molecules/u.c.). At low and intermediate loadings (Figure 2a−c), one can observe that the cations in SII and SI′ sites are significantly displaced, whereas the shape of the MSD plots for SI cation only suggests small vibrational amplitudes around their mean positions. Inspection of both of the trajectories confirms that the SII cations are displaced due to interactions with adsorbed carbon dioxide and move from their initial positions toward the center of the supercage where they are interacting with oxygen atoms near SIII′ sites and

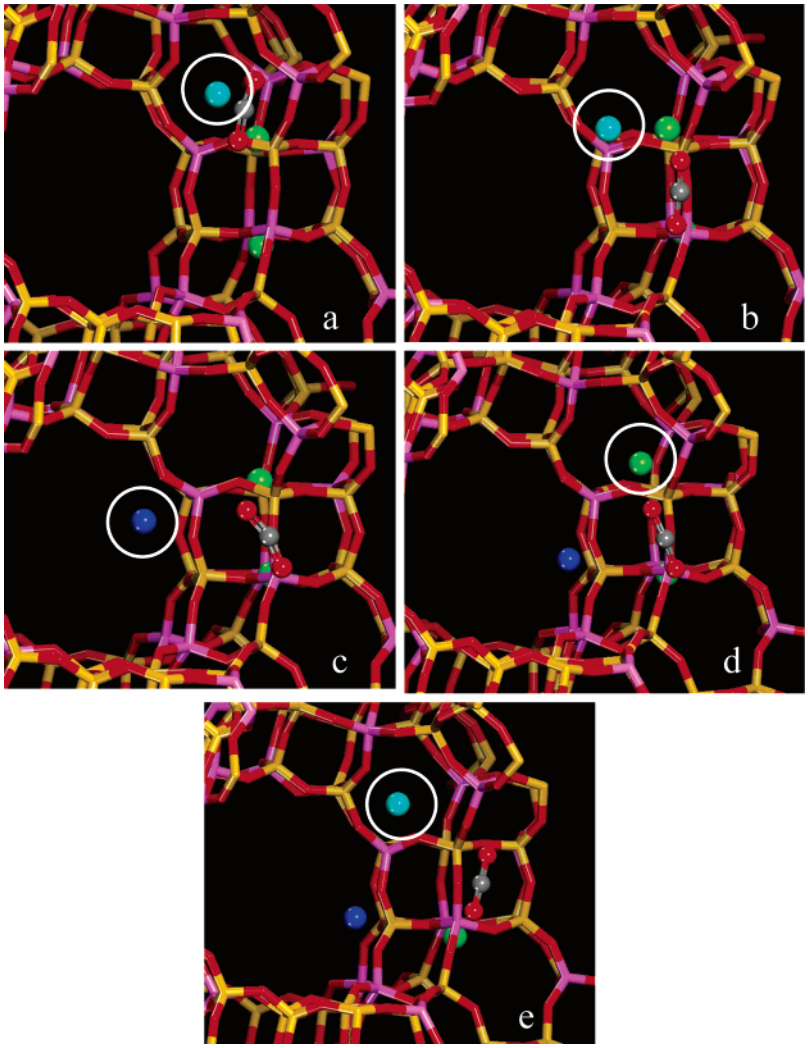

Figure 4. A typical series of images showing a concerted cation motion in NaY. SI′ and SII cations are initially represented in green and light blue respectively (a). Motion of the SII cation to a SIII site represented in dark blue (a−c). Hopping of the SI′ cation into a vacant SII position in the supercage (c−e). Panels b and d correspond to intermediate configurations. For sake of clarity, the circles reported in the various figures highlight the cations involved in the migration process.

adsorbate molecules. This behavior can be confirmed by the shape of the MSDs for the SII cations (Figure 2), suggesting a diffusional type of motion in the supercage associated with a low-energy barrier, since no six-ring window needs to be traversed.This SII to SIII′ displacement is followed by the hopping of SI′ cations from the sodalite cage into the supercage to fill the vacant SII sites. This is illustrated in the RDF for the Na^+(SI′)−O(CO_2) (Figure 3b), where one peak centered around 2.4 Å appears which can only be assigned to the cations interacting with the carbon dioxide molecules within the supercage as the adsorbate molecules cannot access the sodalite cages. In this case, the shape of the MSDs for the SI′ cations is consistent with short hop across a six-ring window corresponding to short time scale events. The most significant example is in Figure 2c, where after 300 ps, the SI′cation motion is only restricted to thermal vibrations which could be due to the absence of vacant neighbor SII sites or SI′ sites within the same sodalite cages. Although this type of SI′−SII motion requires the cation to pass through a zeolite six ring with a high activation barrier, this result is not so surprising, as it has been already observed upon the adsorption of halocarbons[21,25] and methanol[42] with a sequence of SI′−SII′−SII hops. Such cation hopping is consistent with recent data obtained by dielectric relaxation spectroscopy on "dry" NaY, which shows that the SII cation

TABLE 2: Summed *n*(*r*) Values Calculated from the RDFs Reported in Figure 3a,b for NaY[a]

loading	*n*(*r*) SII−O_m	*n*(*r*) SI−O_m
25	0.712	0.090
50	1.348	0.279
71	1.598	0.298
92	2.315	0.328

[a] The integrations are calculated from 0 to 3.00 Å for both SII and SI′ cations corresponding to the first coordination sphere around the cation.

site is more stable than SI′ site.[43] One observes that when the loading increases from 25 to 71 CO_2 /u.c., a larger number of SI′ and SII cations are involved in the aforementioned migration mechanism. The resulting vacant positions are filled by migrating SI′ cations, as suggested by the growing peak centered around 2.4 Å (Figure 3b) and the increase of the summed *n*(*r*) values reported in Table 2, corresponding to the integration of this peak between 0 and 3 Å. An illustration of these cation displacements is provided in Figure 4 obtained for the case of 50 CO_2 molecules per unit cell. The cation initially located in the SII site (Figure 4a) is de-trapped by the presence of the adsorbate molecules, passing through an intermediate state (Figure 4b) before being held in a new position which is close to the SIII′ site (Figure 4c). The so-created SII vacant position

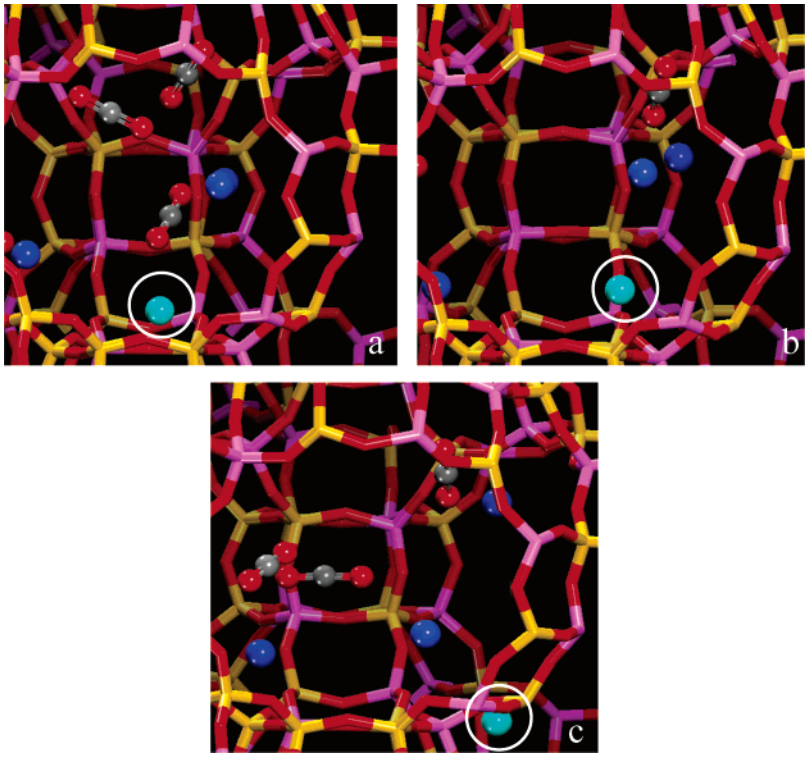

Figure 5. A typical series of images showing a single cation motion in NaY from SII site (a) to SIII′ site (c). Panel b corresponds to an intermediate configuration between the initial and final states. For sake of clarity, the circles reported in the three figures highlight the initial SII cation during its migration to a SIII′ site.

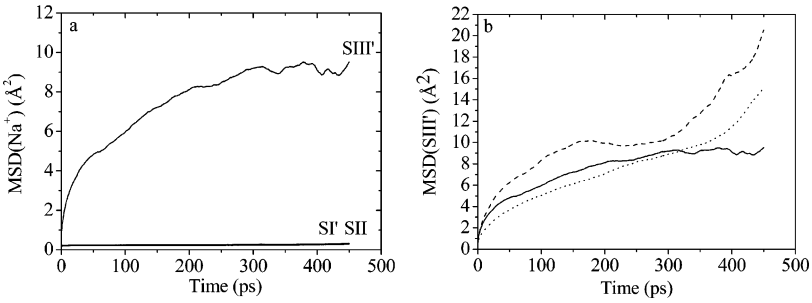

Figure 6. (a) Mean square displacement (MSD) plots for the SI′, SII, and SIII′ cations in NaX at 400 K and at a loading of 21 carbon dioxide molecules per unit cell. (b) MSD plots for the SIII′ as a function of the loading for 21 (solid lines), 42 (dashed lines), and 78 (dotted lines) carbon dioxide molecules per unit cell.

promotes the migration of the SI′cation (Figure 4c−e). A typical single SII cation motion can also occur which is illustrated in Figure 5. It is shown that first, one adsorbed carbon dioxide molecule drags the cation initially located in a SII site (Figure 5a) out of the six-ring window into an intermediate position within the supercage (Figure 5b) before moving it to an SIII′ site. At high loading (92 CO_2 molecules/u.c.), the MSD plot (Figure 2d) suggests that the SI cations are slightly displaced but are not involved in migration through the supercage, as is clearly indicated by the absence of a peak in the RDF for Na^+(SI)−O(CO_2) in the region of 2−3 Å (Figure 3c). Analysis of the trajectories confirms these findings showing rare cases where the SI cations hop out of the double six-ring prism into vacant SI′ sites. The observation of such a cation motion sequence (SI′ to SII, SI to SI′) agrees with the experimental data on "dry" NaY, which shows that the "stability" of the cation sites increases in the series SII > SI′ > SI.[43] Furthermore, the results reported in Table 2 clearly show that the SII cations can coordinate in average up to 2.3 CO_2 in their first environment at high loading, corresponding to the RDF

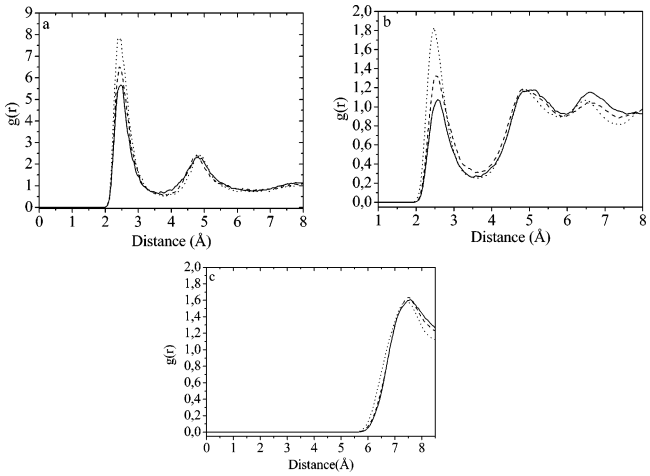

Figure 7. Radial distribution functions (RDFs) (a) Na^+(SIII′)−O(CO_2), (b) Na^+(SII)−O(CO_2), and (c) Na^+(SI′)−O(CO_2) for 21 (solid lines), 42 (dashed lines), and 78 (dotted lines) carbon dioxide molecules per unit cell, calculated at 400 K for NaX/ CO_2 system.

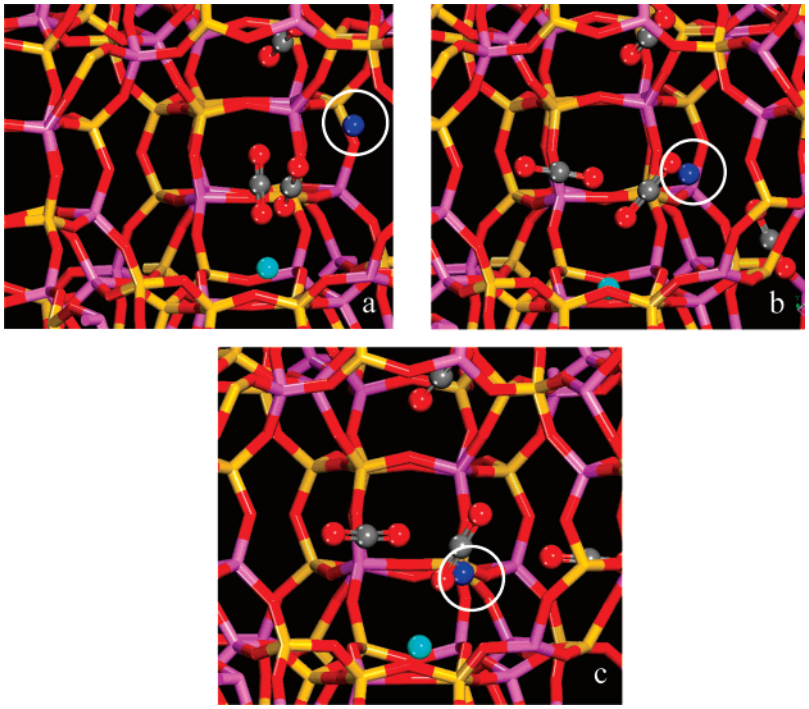

Figure 8. A typical picture showing a single cation motion in NaX from SIII′ (a) to SIII′ (c). The SII and SIII′ cations are represented in light and dark blue, respectively. Panel b corresponds to an intermediate configuration between the initial and final states. For sake of clarity, the circles reported in the three figures highlight the initial SIII′ cation during its migration to another SIII′ site.

TABLE 3: Summed *n*(*r*) Values Calculated from the RDFs Reported in Figures 8A and 8b for NaX[a]

loading	$n(r)$ SIII−O_m	$n(r)$ SII−O_m
21	1.043	0.160
42	1.417	0.393
78	2.300	0.885

[a] The integrations are calculated in both cases from 0 to 3.00 Å.

peak for Na^+(SII)−O(CO_2) in Figure 3a showing an average distance centered around 2.4 Å. These dynamic and geometric obtained data are in very good agreement with our previous grand canonical Monte Carlo[29] and density functional theory[44] simulations, where it was shown that the majority of the SII cation is surrounded by two CO_2's, a few fraction being solvated by three adsorbates.

Figure 6a shows the MSD plots for the SI′, SII, and SIII′ cations in NaX at low loading (21 CO_2 molecules/u.c). One can observe that the SIII′ cations are significantly displaced, whereas SI′ and SII cations remain located in their initial positions. This general behavior is observed at each investigated loading. This result can be explained by the fact that the SIII′ cations are the preferential adsorption sites, as confirmed by the RDF for Na^+ (SIII′)−O(CO_2) (Figure 7a) and the corresponding summed $n(r)$ reported in Table 3. In this table, it is clearly shown that the coordination of SII cation between 0 and 3 Å is very limited, whatever the loading compared to those obtained for the SIII′ site. The carbon dioxide molecules tend to de-trap these cations more easily due to their lower coordination to the oxygen of the zeolite framework when compared to cations at the SII sites. The MSD plot in Figure 6b shows that the mobility of the SIII′ cations is greatest for 42 CO_2/u.c. and then decreases for higher loadings (78 CO_2/u.c.). The shape of all the MSD plots suggests rather the existence of short-range hops between two neighbor SIII′ sites than diffusional type of motion in the supercage. It has to be mentioned that the mobility of SIII′ cations in NaX (Figure 6b) is higher than those of the SII cations in NaY (Figure 2) for a given loading. In addition, the SII cations in NaX are not displaced upon the whole adsorption process even when they start to be coordinated at high loading by a small fraction of surrounding carbon dioxide molecules (Figure 7b, Table 2). Indeed, no vacant SII sites are available thus avoiding the migration of SI′ cations through the six-ring windows which was previously mentioned concerning the NaY system. The RDF for Na^+ (SI′)−O(CO_2) (Figure 7c) confirms this finding with the total absence of a peak in the domain of 2−3 Å. The analysis of the trajectories shows that the SIII′ cations migrate out of their original positions into nearby SIII′ sites upon coordination of the adsorbate molecules. A typical illustration is provided in Figure 8, where it can observed that a carbon dioxide molecule de-traps a SIII′ cation (Figure 8a) to an intermediate position (Figure 8b) before migrating to another SIII′ site (Figure 8c).

4. Conclusion

Molecular dynamics performed on a large time scale was revealed to be a powerful tool for studying the cation redistribution upon the adsorption of carbon dioxide in NaY and NaX Faujasite systems. A concerted migration mechanism has been suggested for NaY. It involves the motion of SII cations toward the center of the supercage leading to vacant SII positions which are then filled by former SI′ cations diffusing through the six-ring windows. At high loading, the SI cation is then allowed to migrates into the nearby SI′ free site. Single cation rearrangements were also observed, leading to displacements of SII cations to vacant SIII′ sites. For NaX, only the SIII′ cations are moved upon adsorption due to accessible location which makes them preferentially coordinated to the adsorbate molecules. It was thus shown that the SIII′ cations migrate out of their original positions into nearby vacant SIII′ sites. This contribution suggests that the motions of the cations when one models the adsorption and diffusion processes in such materials should be considered carefully to gain further understanding of the microscopic mechanisms.

Acknowledgment. This work was supported by EU funding via FP6-Marie Curie Research Training Network "INDENS" (MRTN-CT-2004-005503).

References and Notes

(1) Kikuchi, R. *Energy Environ.* **2003**, *14* (4), 383.
(2) Meier, W. M.; Olson, D. H. Atlas of Zeolite Structures, in *Structure Commission of the International Zeolite Association*; Elsevier: Amsterdam, 1978.
(3) Siriwardane, R. V.; Shen, M. S.; Fisher, E. P.; Poston, J. A.; *Energy Fuels* **2001**, *15*, 279.
(4) Goj, A.; Sholl, D. S.; Akten, E. D.; Kohen, D. *J. Phys. Chem. B* **2002**, *106*, 8367.
(5) Maurin, G.; Llewellyn, P. L.; Poyet, Th.; Kuchta, B. *J. Phys. Chem. B.* **2005**, *109*, 125.
(6) Savitz, S.; Myers, A. L.; Gorte, R. J. *Microporous Mesoporous Mater*. **2000**, *37*, 33.
(7) Siriwardane, R. V.; Shen, M. S.; Fisher, E. P.; Poston, J. A.; *Energy Fuels* **2001**, *15*, 279.
(8) Jacobs, P. A.; Van Santen, R. A. *Stud. Surf. Sci. Catal A* and *B* **1989**, *49*.
(9) Ruthven, D. M.; Shamasuzzaman, F.; Knaebel, K. S. *Pressure Swing Adsorption*; VCH Publishers: New York, 1994.
(10) Harlick, P. J. E.; Handan Tezel, F. *Microporous Mesoporous Mater*. **2004**, *76*, 71.
(11) Bosch, E.; Huber, S.; Weitkamp, J.; Knozinger, H. *Phys. Chem. Chem. Phys*. **1999**, *1*, 579.
(12) Calero, S.; Dubbeldam, D.; Krishna, R.; Smit, B.; Vlugt, T. J. H.; Denayer, J. F. M.; Martens, J. A.; Maesen, T. L. M. *J. Am. Chem. Soc*. **2004**, *126*, 11377.
(13) Maurin, G.; Bell, R.; Devautour, S.; Giuntini, J. C.; Henn, F. *J. Phys. Chem. B* **2004**, *108*, 3739.
(14) Devautour, S.; Abdoulaye, A.; Giuntini, J. C.; Henn, F. *J. Phys. Chem. B* **2001**, *105*, 9297.
(15) Beauvais, C.; Boutin, A.; Fuchs, A. H. *Chem. Phys. Chem*. **2004**, *5*, 1791.
(16) Norby, P.; Poshni, F. I.; Gualtieri, A. F.; Hanson, J. C.; Grey, C. *J. Phys. Chem. B* **1998**, *102*, 839.
(17) Shirono, K.; Endo, A.; Daiguji, H. *J. Phys. Chem. B* **2005**, *109*, 3446.
(18) Pichon, C.; Palancher, H.; Lynch, J.; Hordeau, J. L.; Berar, J. F. *Stud. Surf. Sci. Catal. A* and *B* **2005**, *158*, 789.
(19) Faux, D. A. *J. Phys. Chem. B* **1998**, *102*, 10658.
(20) Lee, Y.; Vogt, T.; Hriljac, J. A.; Parise, J. B.; Hanson, J. C.; Kim, S. J. *Nature* **2002**, *420*, 485.
(21) Grey, C. P.; Poshni, F. I.; Gualtieri, F.; Norby, P.; Hanson, J. C.; Corbin, D. R. *J. Am. Chem. Soc*. **1997**, *119*, 1981.
(22) Sanchez-Sanchez, M.; Blasco, T.; Rey, F. *Phys. Chem. Phys. Chem*. **1999**, *1*, 4529.
(23) Mellot-Draznieks, C.; Rodriguez-Carvajal, J.; Cox, D. E.; Cheetham, A. K. *Phys. Chem. Chem. Phys*. **2003**, *5*, 1882.
(24) Jaramillo, E.; Grey, C. P.; Auerbach, S. M. *J. Phys. Chem. B* **2001**, *105*, 12319.
(25) Ramsahye, N. A.; Bell, R. G. *J. Phys. Chem. B* **2005**, *109*, 4738.
(26) Plant, D. F.; Jobic, H.; Llewellyn, P. L.; Maurin, G. *J. Phys. IV*, in press.
(27) Plant, D. F.; Jobic, H.; Llewellyn, P. L.; Maurin, G. Manuscript submitted for publication.
(28) Kärger J.; Pfeifer, H.; Stallmach F.; Feoktistova N. N.; Zhdanov S. P. *Zeolites* **1993**, 13, 50.
(29) Maurin G.; Llewellyn P. L.; Bell, R. G. *J. Phys. Chem. B* **2005**, *109*, 16084.
(30) Dunne, J. A.; Mariwala, R.; Rao, M.; Sircar, S.; Gorte, J.; Myers, A. L. *Langmuir* **1996**, *12*, 5888.
(31) Khelifa, A.; Derriche, Z.; Bengueddach, A. *Microporous Mesoporous Mater*. **1999**, *32*, 199.
(32) Shen, D.; Bülow, M. *Micropor. Mesopor. Mater*. **1998**, *22*, 237.
(33) Lowenstein, W. *Am. Mineral*. **1954**, *39*, 92.
(34) Fitch, A. N.; Jobic, H.; Renouprez, A. *J. Phys. Chem.* **1986**, 90, 1311.
(35) Zhu; L., Seff; K. *J. Phys. Chem. B* **1999**, *103*, 9512.
(36) Gale, J. D.; *J. Chem. Soc., Faraday Trans.* **1997**, 93, 629.
(37) *Cerius2 v. 4.2*; Accelrys, Inc.: San Diego, 1999.
(38) Maurin, G.; Bell, R. G.; Kuchta, B.; Llewellyn, P. L.; Poyet, Th. *Adsorption* **2005**, *11*, 331.
(39) Plant, D. F.; Maurin, G.; Deroche, I.; Llewellyn, P. L. *Microporous Mesoporous Mater*., submitted for publication.
(40) Smith, W.; Forester, T. R. *J. Mol. Graphics* **1996**, 14, 136.
(41) Frenkel, D.; Smit, B. *Understanding Molecular Simulation*; Academic Press: New York, 1996.
(42) Maurin, G.; Plant, D. F.; Bell, R. G. *J. Phys. Chem. B*, in press.
(43) Devautour-Vinot, S. et al. Manuscript in preparation.
(44) Plant, D.; Deroche, I.; Gaberova, L.; Llewellyn, P. L.; Maurin, G. *Chem. Phys. Lett*., in press.